Original papers
Nanostructured, nanoscale materials and nanodevices

УДК 546.26-162+544.344.016.5 DOI: 10.17277/jamt.2021.04.pp.247-255

Morphology and structure characteristics of nanoscale carbon materials containing graphene

Evgeny K. Belonogov[a,b]✉, Sergey B. Kushev[a], Sergey A. Soldatenko[a], Tatiana L. Turaeva[a]

[a] *Voronezh State Technical University, 84, 20th ann. of October St., Voronezh 394006, Russian Federation,*
[b] *Voronezh State University, 1, University Sq., Voronezh 394018, Russian Federation*

✉ ekbelonogov@mail.ru

Abstract: A comprehensive study of the nanostructured powders (graphite GSM-2; Taunit-M; thermally expanded graphite (TEG)) by methods of transmission electron microscopy (TEM), scanning electron microscopy (SEM), X-ray diffractometry (XRD), reflection high-energy electron diffraction (RHEED), Raman spectroscopy, was carried out. The experimental XRD halo was interpreted by superimposing theoretical diffraction maxima, and an X-ray amorphous graphite phase was revealed. It was found that the X-ray amorphous phase is characterized by the limiting degree of graphite nanostructuring. From the width of the diffraction rings, the maximum sizes of graphite nanocrystals were estimated, which do not exceed 5 and 10 nm in the [0001] and $[10\bar{1}0]$ directions, respectively. Carbon nanotubes and plates of turbostratic graphene were revealed. The structural and morphological parameters of the nanostructured material "Taunit-M" have been established – multi-walled nanotubes with a diameter of up to 10 nm are combined through an interlayer of X-ray amorphous carbon into flat ribbons up to 40 nm wide. Dark-field TEM images (in reflections of $10\bar{1}0$) revealed moiré patterns that appear on overlapping graphene sheets due to double diffraction of the electron beam. It was found that in thermally expanded graphite, the rotation of graphene sheets ranges from 3 to 4°. Within the graphene sheets, complete dislocations with the Burgers vector $b = 1/2$ were revealed [1010]. The Fourier analysis of moiré images made it possible to determine the mutual orientation of graphene sheets, to reveal regions of multilayer graphene, and to identify turbostratic graphene. It is shown that the combination of RHEED, TEM, and Fourier transformations of periodic contrast of electron microscopic images is a promising approach to the analysis of the substructure and morphology of nanoscale carbon materials containing graphene and other allotropic modifications of carbon.

Keywords: thermally expanded, turbostratic graphite; graphene; substructure; transmission and scanning electron microscopy; reflection high-electron diffraction; X-ray diffractometry; Raman spectroscopy.

For citation: Belonogov EK, Kushev SB, Soldatenko SA, Turaeva TL. Morphology and structure characteristics of nanoscale carbon materials containing graphene. *Journal of Advanced Materials and Technologies*. 2021;6(4):247-255. DOI: 10.17277/jamt.2021.04.pp.247-255

Характеристика морфологии и структуры наномасштабных углеродных материалов, содержащих графен

Е. К. Белоногов[a,b]✉, С. Б. Кущев[a], С. А. Солдатенко[a], Т. Л. Тураева[a]

[a] *Воронежский государственный технический университет,*
ул. 20-летия Октября, 84, Воронеж 394006, Российская Федерация;
[b] *Воронежский государственный университет,*
Университетская площадь, 1, Воронеж 394018, Российская Федерация

✉ ekbelonogov@mail.ru

Аннотация: Реализовано комплексное исследование методами просвечивающей электронной микроскопии (ПЭМ), растровой электронной микроскопии (РЭМ), рентгеновской дифрактометрии (РД), дифракции быстрых электронов (ДБЭ), Рамановской спектроскопии наноструктурированных порошков (графит ГСМ-2; «Таунит-М»; терморасширенный графит (ТГ)). Экспериментальное гало РД представлено наложением теоретических дифракционных максимумов, и идентифицирована рентгеноаморфная фаза графита. Установлено, что рентгеноаморфная фаза характеризуется предельной степенью наноструктурирования графита; из ширины дифракционных колец оценены максимальные размеры нанокристаллов графита, которые не превышают

5 и 10 нм в направлениях [0001] и $[10\bar{1}0]$ соответственно. Выявлены углеродные нанотрубки и пластины турбостратного графена. Установлены структурные и морфологические параметры наноструктурированного материала «Таунит-М», многостенные нанотрубки диаметром до 10 нм через прослойку рентгеноаморфного углерода объединены в плоские ленты шириной до 40 нм. На темнопольных ПЭМ изображениях (в отражениях $10\bar{1}0$) выявлены картины муара, которые возникают на перекрывающихся листах графена вследствие двойной дифракции электронного пучка. Установлено, что в ТГ разворот листов графена составляет от 3 до 4°. В пределах листов графена выявлены полные дислокации с вектором Бюргерса $b = 1/2$ [1010]. Методика Фурье образов изображений муара позволила определить взаимную ориентацию листов графена, выявить области многослойного графена и идентифицировать турбостратный графен. Показано, что объединение методов ДБЭ, ПЭМ и Фурье трансформации периодического контраста электронномикроскопических изображений – перспективный подход к анализу субструктуры и морфологии наномасштабных углеродных материалов, содержащих графен и другие аллотропные модификации углерода.

Ключевые слова: терморасширенный, турбостратный графит; графен; субструктура; просвечивающая и растровая электронная микроскопия; дифракция быстрых электронов; рентгеновская дифрактометрия; Рамановская спектроскопия.

Для цитирования: Belonogov EK, Kushev SB, Soldatenko SA, Turaeva TL. Morphology and structure characteristics of nanoscale carbon materials containing graphene. *Journal of Advanced Materials and Technologies*. 2021;6(4):247-255. DOI: 10.17277/jamt.2021.04.pp.247-255

1. Introduction

The increased interest in graphene is due to its unusual physical properties and various options for its practical application. Today, a large number of methods for preparing graphene are known, but the problem of producing defect-free graphene on various substrates for practical use in commercial quantities remains relevant.

In accordance with the terminology described in [1], graphene is an ordered one-layer two-dimensional hexagonal structure formed by bonded carbon atoms in sp^2-hybridization. The graphene derivatives are highlighted in the classification. Turbostratic graphite (TG) is a two- or three-layer graphene, in which individual layers can be connected either by the type of a regular HCP lattice, or unfolded relative to each other in an arbitrary manner relative to an axis perpendicular to the graphene layers. Multilayer graphene is a layered carbon structure containing from 2 to 10 graphene layers, in which the layers can be in the same mutual orientations as in turbostratic graphite. Exfoliated graphite is a material up to 100 nm thick obtained by mechanical, thermal (thermo-expanded) or chemical exfoliation of graphite. The distance between graphene layers in graphite is approximately 0.335 nm, the sp^2 carbon-carbon bond length in graphene is 0.142 nm [2]. Graphene can exist on substrates, such as sols, or in a free state.

Synthesis methods

There are two groups of graphene synthesis methods [3]: descending and ascending. The first group of methods includes: micromechanical cleavage (using adhesive tape or an atomic force microscope (AFM) tip), chemical cleavage and chemical synthesis (using ultrasound and reduction of graphene oxide). Micromechanical cleavage – capture of thin graphite flakes or AFM tip by the adhesive surface of an adhesive tape; allows obtaining multiple layers and single-layer graphene with multiple repetitions. The use of pyrolytic graphite and adhesive polymer made it possible to obtain single-layer graphene with transverse dimensions up to 10 μm [4].

The Hammer method (dispersion of graphene in solvents) is characterized by a good yield and low cost, based on the oxidation of graphite powders with oxidants (H_2SO_4; $KMnO_4$; $NaNO_3$) to graphite oxide, followed by exfoliation of the graphene oxide by ultrasound in water. Methods for the reduction of graphene from oxide are: chemical [5, 6], thermal [7] and microwave [8]. Microwave and thermal approaches have a negative impact on the quality of graphene due to the temperature gradient. Modification of graphene with different functional chemical groups can uncontrollably change its properties and limit the scope of application.

In the method of liquid-phase exfoliation, graphene exfoliates in liquid media using ultrasound or shear forces of a different nature [9]. The growth and subsequent destruction of bubbles during exposure lead to the exfoliation of graphite to several layers of graphene; the pressure drop also contributes to the graphite cleavage.

The specific energy of surface interaction between graphene layers is $4.67 \cdot 10^{-2}$ J·m^{-2} [10]. For delamination, a liquid-phase medium should be used, in which the surface tension energy is close to

the surface interaction energy of the graphite layers [11]; this requirement is met by N,N-dimethylformamide ($3.71 \cdot 10^{-2}$ J·m^{-2}) and N-methylpyrrolidone ($4.01 \cdot 10^{-2}$ J·m^{-2}) [12, 13], but they are toxic, expensive and have a high boiling point. The authors of [14, 15] use solvents with a low boiling point (isopropyl alcohol, ethanol, acetone, methanol, and acetonitrile). Water is also a good solvent (surface tension $7.21 \cdot 10^{-2}$ J·m^{-2}); surfactants are added to water to reduce surface tension.

To obtain graphene in the form of a film on a substrate, the method of electrochemical exfoliation is used [16]. As a working electrode, graphite rods, pyrolytic or natural graphite are used, and as electrolytes, ionic liquids (LiCl, $LiClO_4$ in propylene carbonate, LiCl in dimethyl sulfoxide) or aqueous solutions (H_2SO_4, $(NH_4)_2SO_4$) [17]. As the second electrode, foils of chemically resistant metals are used, the electric potential is from –10 to +10 V. The exfoliation process usually occurs on the positive electrode, which is oxidized, and negative ions from the solution are incorporated into the graphite layers.

Mechanical grinding of graphite is a simple, effective method, with the process being controlled by the main parameters [18]. To obtain a colloidal dispersion of graphene, organic solvents (acetone, formamide, and tetrahydrofuran) are used. In general, when using top-down methods, it is difficult to obtain graphene in the form of large-area films.

Basic bottom-up methods are epitaxial growth of graphene on a substrate (surfaces with 60° symmetry are used) by chemical vapor deposition; pyrolysis; chemical vapor deposition. The most promising are chemical vapor deposition and thermal decomposition of silicon carbide in ultrahigh vacuum. In the thermal decomposition of SiC, it is used both as a starting material and as a substrate material. During the thermal decomposition of SiC, carbon is already present on the substrate, while during chemical deposition it comes from the gas phase. The properties of epitaxial graphene depend on the size of the mismatch between the crystal lattices of graphene and the substrate. At present, theoretical and experimental studies of the graphene structure on the surfaces of 111 FCC metals (Cu, Au, Ni, Pt, Rh, Ir), on the surfaces of metals 0001 with a hexagonal crystal lattice (Re, Co, Ru), and also on 0001 SiC are known [19, 20]. A characteristic feature of the structure of graphene obtained on metal surfaces is a high density of defects at grain boundaries. In [19], the mechanisms of nucleation (homogeneous, heterogeneous) and growth of graphene islands were considered. In the case of homogeneous nucleation, the stability of graphene nuclei depends on the temperature and concentration of migrating carbon atoms. In the case of heterogeneous nucleation, an increase in the growth rate is observed in the presence of surface defects.

The review [21] considers the main results obtained during the growth of graphene by chemical vapor deposition. Low-defect graphene layers were grown on a Si substrate with a Ni sublayer at a temperature of 970 °C, on the surface of a Cu–Ni alloy at a temperature of 750 °C. High quality graphene was grown on copper foil in the temperature range from 650 to 850 °C. The use of methane CH_4 as a carbon source is usually problematic as the density of the deposited graphene increases with increasing layer thickness. The quality of the obtained graphene on copper foil is higher than on other metals due to the low solubility of carbon in copper. The authors of [22] investigated the influence of the topographic features of copper foil Cu substrates, polycrystalline Cu films, and epitaxial Cu films on the morphology of the resulting graphene layers.

Characterization methods

Graphene is identified by AFM and Raman spectroscopy [23, 24]. AFM allows the determination of layers in multilayer graphenes. Problems with this method arise due to the high adsorption capacity of graphene. Single-layer graphene is usually characterized by a thickness of 0,6 – 1 nm, but the measured thickness of single-layer graphene on a SiO_2 substrate using AFM exceeds the expected one by a factor of 2 – 3 [25]. In addition, the accuracy of the results depends on the type of substrate and the method of sample preparation [26]. RS is used to characterize hybridized sp^2 and sp^3 carbon atoms. This method is commonly used for studies of single-layer, double-layer and multilayer graphene and can be used to determine the number of graphene layers. In [27], typical Raman spectra of single-layer graphene, graphite, nanostructured graphite, single-wall carbon nanotube, and amorphous carbon were considered. The Raman spectrum is sensitive to deformation of the sp^2 bond and can be used to determine the modifications of graphene [28]. Defects in the graphite lattice lead to resonance spectra, which makes the Raman method sensitive to disorder in carbon materials [29].

There are a few studies of graphene structures by scanning tunneling microscopy (STM) [30], X-ray diffractometry (XRD) [31], scanning electron microscopy (SEM), and transmission electron microscopy (TEM) [15, 31]. One-layer and

multilayer graphene can be observed using STM, but such studies require a rather complex experiment in an ultrahigh vacuum and are not often used to verify graphene. The XRD is used for phase analysis and control of interplanar expansion in graphite and graphene oxide. The XRD allows us to conclude that graphene is present if the 0002 peak of graphite broadens and shifts to the left. The SEM is used to study the morphology of graphene and detect impurities, folds, and damage to graphene layers [15, 32]. The SEM method is ineffective for resolving ultrathin layers.

The results of TEM visualization of graphene layers presented to date are few. The main advances in graphene visualization obtained by TEM are presented in [15] and review [33]. The degree of damage to the sample by the electron beam can be noticeable, but the damage to graphene is not so significant because of its good conductivity.

Sample preparation for TEM

Samples for TEM are prepared by applying a solution (suspension) of dispersed graphene to an electron microscopic grid and subsequent drying. Other methods are also used: mechanical exfoliation of the graphene layer from pyrolytic graphite, natural graphite or graphene on silicon carbide; separation of graphene layers by etching followed by transfer to the grid; electrochemical separation method; method of exothermic reaction with intensive formation of gas bubbles; method of ultrasonic dispersion of graphene suspension.

In order to identify effective approaches to characterizing the substructure, structure, and morphology of nanoscale materials containing graphene and other allotropic modifications of carbon, a comprehensive study of nanostructured carbon materials by TEM, SEM, XRD, reflection high-electron diffraction (RHEED), and Raman scattering methods has been carried out.

2. Materials and methods

2.1. Materials

The following powders were used as objects of research: special low-ash graphite GSM-2 (ZAO "Graphiteservice", Chelyabinsk, Russia); carbon material "Taunit-M" and thermally expanded graphite (TEG) (LLC "NanoTechCenter", Tambov, Russia).

2.2. Characterization methods

The phase composition of carbon nanomaterials was monitored by XRD on an ARL X'TRA diffractometer (Thermo Fisher Scientific, Switzerland), a wavelength of 0.15406 nm and RHEED on an EG-100M electronograph (SZEM, Sumy, USSR). The study of the surface morphology and the elemental composition of the powder was carried out by the SEM method on a JSM-6380 scanning electron microscope (JEOL, Japan) with an INCA Energy 250 X-ray energy dispersive analysis system. The analysis of the substructure of the samples was carried out by the TEM method on a Libra-120 transmission electron microscope (Carl Zeiss; Germany). For TEM, the samples were prepared by ultrasonic dispersion on an UZDN-2T device (Amtorg LLC, Belgorod, Russia) of the test material in distilled water until a suspension was formed, then the suspension was placed on an electron microscopic grid covered with an amorphous carbon film transparent to the electron beam.

3. Results and Discussion

Figure 1 shows the results of XRD study of crystalline graphite GSM-2 and nanostructured carbon material "Taunit-M". It was found that GSM-2 crystallites have an atomic structure of a hexagonal lattice P63 / mmc with $a = b = 0.2456$ nm and $c = 0.6709$ nm. A slight broadening was observed only for peaks 0002 and 0004 (see Fig. 1*a*); the degree of graphitization is 0.98 – 1, i.e. the graphite structure is perfect.

The diffractogram for "Taunit-M" (see Fig. 1*b*) has a halo characteristic of an X-ray amorphous material. The profile of the experimental halo can be theoretically depicted by adding (superimposing) two diffraction maxima, one of which corresponds to the crystal lattice of perfect graphite, and the second is a broad peak 0002 of graphite shifted "to the left", i.e. indicating an increase in parameter c. Thus, the XRD results indicate the presence of a substantial fraction of X-ray amorphous graphite in the Taunit-M composition, in which the distance between the atomic planes (0002) is increased, which can lead to the formation of graphene flakes.

Figure 2 shows the results of TEM studies of the nanostructured carbon material "Taunit-M". The same figure shows electron diffraction patterns (microdiffraction mode) obtained in the aperture of the selector diaphragm from the selected area of the sample. The morphology and substructure of the material is characterized by a disordered conglomeration of filamentous, ribbon-like, and leaf-like fragments, as a rule, substantially deformed. Fragment of a microdiffraction pattern (see Fig. 2*a*) indicates an X-ray amorphous phase of filament and ribbon-like fragments, i.e. Taunit-M is characterized

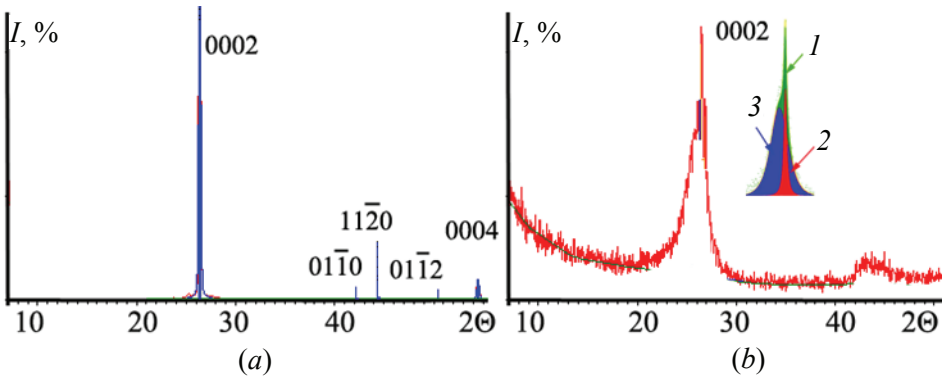

Fig. 1. Fragments of diffraction patterns of the graphite GSM-2 (*a*) and "Taunit-M" (*b*):
1 – experimental halo profile; *2* – diffraction maximum of perfect graphite; *3* – broad 0002 graphene peak

by the extreme degree of nanostructuring. Based on the widths of the diffraction rings 0002, $10\bar{1}2$, and $11\bar{2}0$, one can estimate the maximum sizes of nanocrystals, which do not exceed 5 and 10 nm in the [0001] and $[10\bar{1}0]$ directions, respectively.In the TEM image, ribbons and filaments are no more than 40 nm wide, 10 nm thick and unlimited in length. In the direction of the length of the tape, there is a continuous contrast with the morphology of the filaments. From the established morphological parameters, it can be assumed that the observed filaments are multi-walled nanotubes up to 10 nm in diameter, and several nanotubes are combined through an interlayer (amorphous carbon) into flat ribbons. A fragment of the microdiffraction pattern (see Fig. 2*b*) characterizes the phase composition and spatial orientation of thin carbon crystals. The indexing of the electron diffraction pattern unambiguously indicates the location of the (0001)

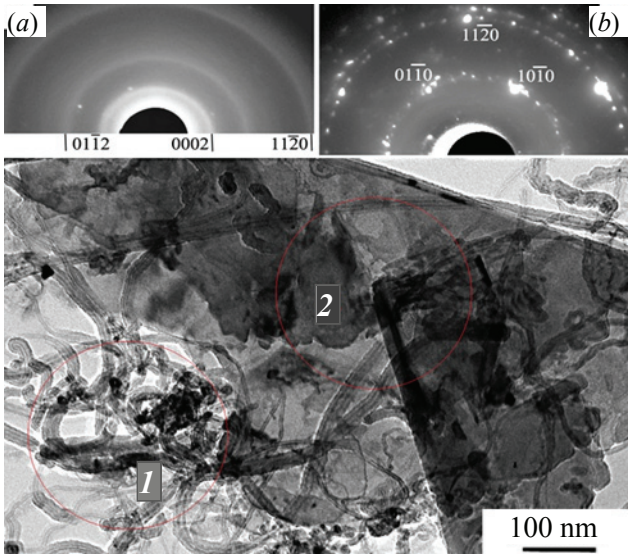

Fig. 2. TEM image of the "Taunit-M" carbon material:
a – electron diffraction pattern from section *1*,
b – electron diffraction pattern from section *2*

plane of graphite in the plane of observation of the sample in transmission in the RHEED mode.

Obviously, extended (with lateral dimensions of 1 μm and more) flat fragments are graphene sheets. Since the microdiffraction pattern from a region (region *2* in Fig. 2) with an area of no more than $7 \cdot 10^4$ nm^2 shows several RHEED patterns for the [0001] zone axis of the graphite lattice, it can be concluded that, in addition to large graphene sheets, the studied region of the sample contains smaller flakes with the zone axis [0001], but arbitrarily deployed in azimuth. Thus, TEM and RHEED showed that Taunit-M contains a noticeable fraction of carbon nanotubes and turbostratic graphene sheets.

Figure 3 shows the general (from the sample area more than 10^4 μm^2) electron diffraction pattern, which gives an integral estimate of the TEG phase composition. Analysis of the general diffraction patterns obtained by the RHEED method and the data on the elemental composition made it possible to identify, in the main, two phases in the TEG powder: crystalline graphite; X-ray amorphous graphite. At the same time, the integral assessment of the diffraction maxima in the electron diffraction pattern (see Fig. 3) showed that the intensities of the $10\bar{1}0$ and $11\bar{2}0$ peaks $10\bar{1}0$ are extremely high, and the 0002 peak is absent. This is possible only under the condition that the overwhelming proportion of the flakes transparent to the electron beam of the electron diffraction device is located by the (0001) plane in the plane of the electron microscopic grid. Note that the diffraction maxima are extremely narrow, which indicates a crystalline perfection at a large distance in the lateral directions of the crystal planes $10\bar{1}0$ and $11\bar{2}0$. Thus, the RHEED results indicate the presence of a significant fraction of graphene flakes in the TEG composition.

Figure 4 shows a TEM image of TEG particles, which was obtained in the "dark field" mode, namely, in a diffracted beam $10\bar{1}0$.

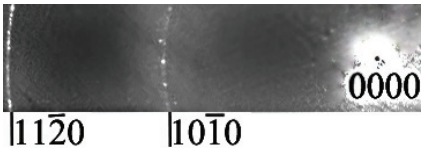

Fig. 3. TEG electron diffraction pattern (general diffraction)

The corresponding TEM image in the "bright field" mode (in a strong transmitted beam) has a weak contrast due to the small atomic scattering factor of carbon. According to light- and dark-field TEM images, TEG consists of deformed graphene sheets and contains well-faceted graphite single crystals with sizes ranging from 100 to 150 nm. The revealed submicron graphite single crystals are of separate methodological interest; perfect crystals of graphite of submicron size, apparently, remnants of blocks of initial graphite, in which the intercalation of ions did not take place upon interaction with acids. According to [34], the introduction of anions into a graphite layer occurs through surface defects of a single crystal of graphite; therefore, defect-free regions are the most resistant to the intercalation process.

Within the overlapping crumpled graphene sheets are distributed particles of carbon and crystalline graphite with a size of dispersion from 2 nm to 250 nm. The most significant fraction is hexagonal prismatic graphite particles with crystallographic faceting along the planes (0001), $(10\bar{1}0)$, $(10\bar{1}1)$ and $(11\bar{2}2)$. Comparing the results of SEM and TEM, we can conclude that the sizes of graphite TEG particles are in the range from 20 nm to 10 μm. It is most likely that larger particles can consolidate smaller ones. Regular moiré patterns in active reflections $10\bar{1}0$, resulting from double diffraction on overlapping blocks, are well manifested in dark-field images (Figure 4), which indicates a fairly perfect hexagonal structure of graphene blocks.

Within individual graphene sheets, the moiré period ranges from 3 to 4 nm, which corresponds to the mutual rotation of sheets by 4° and 3°, respectively.

Moiré patterns within graphene sheets reveal single complete dislocations with the Burgers vector $b = 1/2$ [1010], lying in the basal plane (0001). The contrast inhomogeneity is apparently caused by extinction (bending and deformation), as well as by the presence of nanocrystalline and X-ray amorphous phases (based on carbon), which are distributed over graphene sheets.

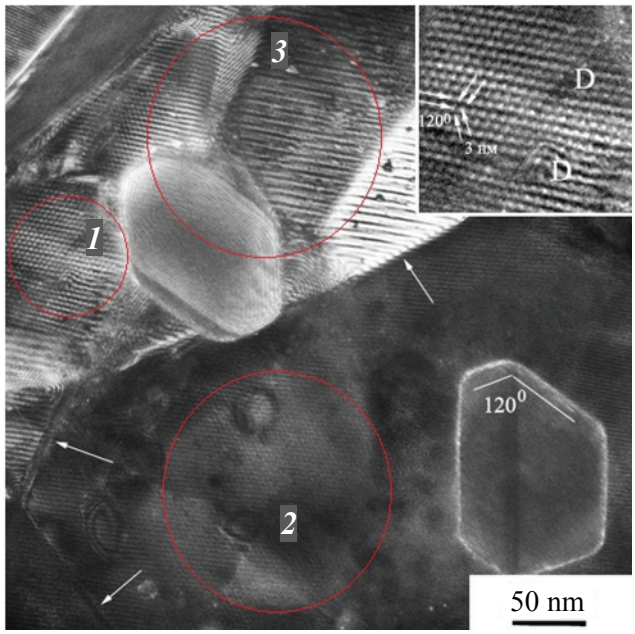

Fig. 4. TEM image of the TEG ("dark field" mode in a $10\bar{1}0$beam): arrows indicate the boundaries of graphene sheets; the inset shows a fragment of a moiré image showing the directions of the lines, the moiré period, and the position of dislocations (D)

Moiré patterns were analyzed using the Fourier transform of TEM images. Fig. 5 shows the Fourier transforms of the TEM image fragments designated as *1*, *2*, and *3* in Fig. 4. The Fourier images of the moire patterns in Fig. 4 illustrate a TEM image of moiré, revealing the substructure of a graphene-based material in exfoliated graphite. The Fourier transform (Fig. 5*a*) shows the hexagonal regions of multilayer graphene, i.e. identify turbostratic graphene sheets. The turbostratic graphene manifests itself in RHEED patterns and Fourier patterns by a deviation from the 60-degree symmetry of reflections, when, instead of 6 reflections (for AB packing of the HCP lattice) of graphene, several orders of magnitude appear (6, 12, etc.), and the angle of rotation of the reflections corresponds to the angle of mutual orientation of graphene layers (see Figs. 5*b*, *c*).

The misaligned arrangement of layers can arise due to the repackaging of layers with different orientations in the processes of flake exfoliation and compaction of nanopowder. It should also be noted that the surface of the flakes is inhomogeneous and the X-ray amorphous phase of carbon is also constantly present.

Figure 6 shows SEM images (in the mode of registration of secondary electrons) of TEG. At low magnifications (Fig. 1*a*), the image contrast reveals the spontaneous compaction of individual particles of the carbon conglomerate into granules up to 50 μm

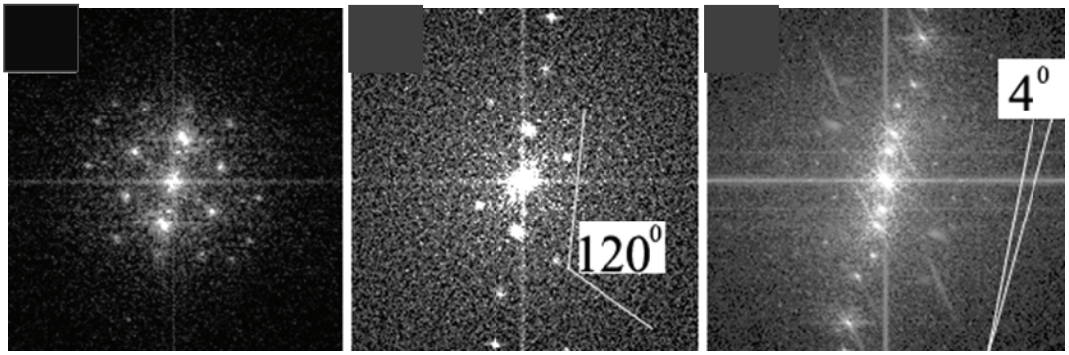

(*a*) (*b*) (*c*)

Fig. 5. Fourier transforms of TEM moiré images formed at the boundaries of graphene sheets: *a*, *b*, *c* – correspond to the fragments of Fig. 3, designated *1*, *2*, *3*, respectively

in size with developed open porosity. Energy dispersive microanalysis revealed that the fraction of C in the powder does not exceed 80 at. %. The content of O, N, S (up to 6 at.% Each) and traces of Ca, Ni, Cu, Zn. Fig. 6*b* illustrates the morphology of an individual powder particle.The contrast reveals multiple crumpled sheets of carbon, which, taking into account the results of the RHEED (see Fig. 3), are very likely turbostratic graphene.

Figure 7 shows the results of the study of carbon nanostructured materials TEG and "Taunit-M" by Raman spectroscopy. It was found that all revealed Raman peaks (except for G) are combined. The survey Raman spectra for TEG and "Taunit-M" have a similar appearance (see Fig. 7*a*).

The G-peak characterizes sp^2 carbon bonds in graphite and graphene. Peak D (1350 cm^{-1}) confirms the high imperfection of the graphite lattice for TEG and Taunit-M. The 2D peak (2680 cm^{-1}) for single-layer graphene, as a rule [28, 29], is more intense and sharper in comparison with multilayer graphene, and is also slightly shifted relative to the peak characteristic of defective graphite. A detailed analysis of the Raman spectrum profile (compare curves *1* and *2* in Fig. 7*b*) allows us to conclude that there is a significant proportion of graphene and turbostratic graphite in TEG and Taunit-M.

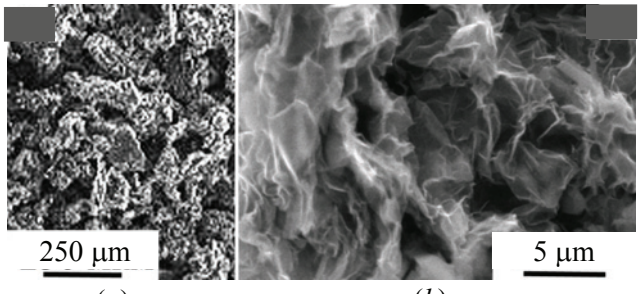

(*a*) (*b*)

Fig. 6. SEM images of the TEG; overview image of the surface of a self-compacted powder (*a*) and morphology of an individual particle (*b*)

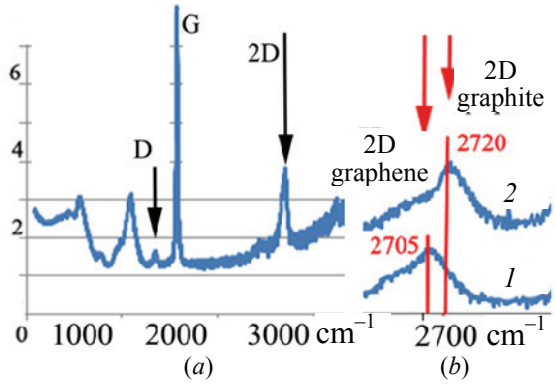

(*a*) (*b*)

Fig. 7. Overview Raman spectrum of the TEG suspensions (*a*) and fragments of spectra (*b*): *1* – thermally expanded graphite; *2* – "Taunit-M"

The RHEED techniques in combination with TEM studies in weak beams, as well as the Fourier transform of periodic contrast (moiré pattern) on TEM images, have shown high efficiency in identifying and analyzing the substructure of X-ray amorphous and nanocrystalline carbon-based materials containing multilayer graphene and other allotropic modifications of carbon.

4. Conclusions

An integrated approach (TEM, SEM, RHEED, XRD, Raman spectroscopy) to characterization of the substructure of materials containing graphene and other allotropic modifications of carbon allows us to formulate a conclusion about the high efficiency and resolution of TEM and RHEED. According to the XRD data, an X-ray amorphous graphite phase was identified in the Taunit-M composition. The efficiency of the XRD technique can be enhanced by analyzing the profile of the experimental halo by superimposing theoretical diffraction maxima corresponding to the crystal lattice of perfect graphite and possible variations in the nanocrystalline and

X-ray amorphous phases. According to TEM data, carbon nanotubes and turbostratic graphene were identified in the Taunit-M composition. The TEG contains a significant proportion of graphene flakes. The efficiency of the TEM technique can be enhanced by analyzing in $10\bar{1}0$ reflections dark-field images (in weak beams) of moiré patterns of overlapping graphene sheets. By measuring the moiré period, it was found that in the TEG the unfolding of graphene sheets is 3–4°. Within the graphene sheets, complete dislocations with the Burgers vector $b = 1/2$ [1010] were revealed. A highly efficient approach – the use of Fourier images of TEM images of moiré, allows one to determine the mutual orientation of graphene sheets; to reveal the hexagonal regions of multilayer graphene, i.e. identify turbostratic graphene. RHEED in combination with TEM and Fourier transformation of periodic contrast in TEM images is the most promising approach to identification and analysis of the substructure of materials based on various allotropic modifications of carbon. SEM and Raman spectroscopy methods act as auxiliary ones. The results of studying "Taunit-M" carbon nanostructured material and TEG by Raman spectroscopy confirmed the data obtained by TEM and RHEED.

The results of this work will be useful to developers of technologies for creating graphene and ultrathin graphite layers for electrodes of lithium-ion power sources. At the stages of manufacture and operation, electrochemical separation of electrodes occurs due to the intercalation of anions into defects in graphite crystallites. This fact makes us look for reliable, high-resolution and reliable methods for controlling the structure and substructure of composite (crystalline and X-ray amorphous) materials based on various allotropic modifications of carbon.

6. Funding

This study was funded by the RFBR grant No. 18-29-11062 MK.

7. Acknowledgements

The authors express their deep appreciation and gratitude to the management of NanoTechCenter LLC (Tambov, Russia) for the research objects provided, Ch. V. Yu. Akhmedov (Voronezh, Russia) for sample preparation of suspensions of carbon materials, associate professor D.L. Goloshchapov and professor P.V. Seredin Voronezh State University (Voronezh, Russia) for technical assistance in the study by the method of Raman scattering.

8. Conflict of interests

The authors declare no conflict of interest.

References

1. Bianco A, Cheng H-M, Enoki T. All in the graphene family – A recommended nomenclature for two-dimensional carbon materials. *Carbon*. 2013;65:1-6. DOI:10.1016/j.carbon.2013.08.038

2. Kuilla T, Yao D, Lee, JH, Bhadra S, Kim NH, Bose S. Recent advances in graphene based polymer composites. *Progress in Polymer Science.* 2010;35(11):1350-1375. DOI:10.1016/j.progpolymsci.2010.07.005

3. Adetayo A, Runsewe D. Synthesis and fabrication of graphene and graphene oxide: A review. *Open Journal of Composite Materials.* 2019;9(2):207-229. DOI:10.4236/ojcm.2019.92012

4. Noorden RV. Production: beyond sticky tape. *Nature.* 2012;483(7389):S32-S33. DOI:10.1038/483S32a

5. Silva KD, Huang HH, Joshi R, Yoshimura M. Chemical reduction of graphene oxide using green reductants. *Carbon*. 2017;119:190-199. DOI:10.1016/j.carbon.2017.04.025

6. Kumari S, Panigrahi A, Singh SK, Pradhan SK. Synthesis of graphene by reduction of graphene oxide using non-toxic chemical reductant. In: J. Chattopadhyay et al. (eds.) *Innovation in Materials Science and Engineering*. Singapore: Springer Nature; 2018. p.143-150. DOI:10.1007/978-981-13-2944-9_14

7. Alam SN, Sharma N, Kumar L. Synthesis of graphene oxide (GO) by modified hummers method and its thermal reduction to obtain reduced graphene oxide (*r*GO). *Graphene.* 2017;6(1):1-18. DOI:10.4236/graphene.2017.61001

8. Han HJ, Chen YN, Wang ZJ. Effect of microwave irradiation on reduction of graphene oxide films. *RSC Advances.* 2015;5:92940-92946.

9. Ullah S, Yang X, Ta HQ, Hasan M, Bachmatiuk A, Tokarska K, et.al. Graphene transfer methods: A review. *Nano Research.* 2021;14(11):3756-3772. DOI:10.1007/s12274-021-3345-8

10. Wang S, Zhang Y, Abidi N, Cabrales L. Wettability and surface free energy of graphene films. *Langmuir.* 2009;25(18):11078-11081. DOI:10.1021/la901402f

11. Hernandez Y, Nicolosi V, Lotya M, Blighe FM, Sun Z, De S, et.al. High-yield production of graphene by liquid-phase exfoliation of graphite. *Nature. Nanotechnology.* 2008;3(9):563-568. DOI:10.1038/nnano.2008.215

12. Jasper JJ. The surface tension of pure liquid compounds. *Journal of Physical and Chemical Reference Data*. 1972;1(4):841-1010. DOI:10.10631/1.3253106

13. Hernandez Y, Lotya M, Rickard D, Bergin SD, Coleman N. Measurement of multicomponent solubility parameters for graphene facilitates solvent discovery. *Langmuir.* 2010;26(5): 3208-3213. DOI:10.1021/la903188a

14. O'Neill A, Khan U, Nirmalraj PN, Boland J, Coleman JN. Graphene dispersion and exfoliation in low boiling point solvents. *Journal of Physical Chemistry C.* 2011;115(13): 5422-5428. DOI:10.1021/JP110942E

15. Celik Y, Flahaut E, Suvac E. A comparative study on few-layer graphene production by exfoliation of different starting materials in a low boiling point solvent. *Flatchem.* 2017;1:74-88. DOI:10.1016/j.flatc.2016.12.002

16. Jibrael RI, Mohammed MK. Production of graphene powder by electrochemical exfoliation of graphite electrodes immersed in aqueous solution. *Optik.* 2016;127(16):6384-6389. DOI:10.1016/j.ijleo.2016.04.101

17. Parvez K, Wu ZS, Li R, Liu X, Graf R, Feng X, et.al. Exfoliation of graphite into graphene in aqueous solutions of inorganic salts. *Journal of the American Chemical Society*. 2014;136(16):6083-6091. DOI:10.1021/ja5017156

18. Ullah M, Ali ME, Hamid SBA. Surfactant-assisted ball milling: a novel route to novel materials with controlled

nanostructure – a review. *Reviews on Advanced Materials Science.* 2014;37(1):1-14.

19. Tetlow H, Boer JP, Ford IJ, Vvedensky DD, Coraux J, Kantorovich L. Growth of epitaxial graphene: Theory and experiment. *Physics Reports.* 2014;542(3):195-295. DOI:10.1016/j.physrep.2014.03.003

20. Yazdi GR, Iakimov T, Yakimova R. Epitaxial graphene on SiC: A review of growth and characterization. *Crystals*. 2016;6(5):53-98. DOI:10.3390/cryst6050053

21. Xu S, Zhang L, Wang B, Ruoff RS. Chemical vapor deposition of graphene on thin-metal films. *Cell Reports Physical Science.* 2021;2(3)100372. DOI:10.1016/j.xcrp.2021.100372

22. Huet B, Raskin JP, Snyder DW, Redwing JM. Fundamental limitations in transferred CVD graphene caused by Cu catalyst surface morphology. *Carbon*. 2020;163:95-104. DOI:10.1016/j.carbon.2020.02.074

23. Comanescu F, Istrate A, Purica M. Assessing by Raman spectroscopy the quality of CVD graphene transferred on oxidized silicon and quartz substrates. *Romanian Journal of Information Science and Technology*. 2019;22(1):30-40.

24. Bautista-Flores C, Sato-Berru RY, Mendoza D. Raman spectroscopy of CVD graphene during transfer process from copper to SiO_2/Si substrates. *Materials Research Express.* 2018;6(1):015601. DOI:10.1088/2053-1591/aae32f

25. Novoselov KS, Geim AK, Morozov SV, Jiang D, Zhang Y, Dubonos SV, et al. Electric field effect in atomically thin carbon films. *Science*. 2004;306(5696):666-669. DOI:10.1126/science.1102896

26. Gubin SP, Tkachev SV. Graphene and materials based on it. *Radioelektronika. Nanosistemy. Informacionnye Tekhnologii*. 2010;2(1-2):99-137. (In Russ).

27. Ziatdinov AM. Raman spectroscopy of nanoscale honeycomb carbon structures. *Vestnik dal'nevostochnogo otdeleniya Rossiyskoy Akademii Nauk*. 2020;(6):27-40. DOI: 10.37102/08697698.2020.214.6.003. (In Russ)

28. Dresselhaus MS, Eklund PC. Phonons in carbon nanotubes. *Advances in Physics.* 2000;49(6):705-814. DOI:10.1080/000187300413184

29. Wu J, Lin ML, Xin C, Liua HN, Tan PH. Raman spectroscopy of graphene-based materials and its applications in related devices. *Chemical Society Reviews.* 2018;47(5):1822-1873. DOI:10.1039/C6CS00915H

30. Palinkas A, Molnar G, Hwang C, Biro LP, Osvath Z. Determination of the STM tip-graphene repulsive forces by comparative STM and AFM measurements on suspended grapheme. *RSC Advances.* 2016;6(89):86253-86258. DOI:10.1039/C6RA19660H.

31. Stobinski L, Lesiak B, Malolepszy A, Mazurkiewicz M, Mierzwa B, Zemek J, et.al. Graphene oxide and reduced graphene oxide studied by the XRD, TEM and electron spectroscopy methods. *Journal of Electron Spectroscopy and Related Phenomena.* 2014;195:145-154. DOI:10.1016/j.elspec.2014.07.003

32. Siburian R, Sihotang H, Raja SL, Supeno M, Simanjuntak C. New route to synthesize of graphene nano sheets. *Oriental Journal of Chemistry*. 2018;34(1):182-187. DOI:10.13005/ojc/340120

33. Bachmatiuk A, Zhao J, Gorantla S, Martinez IG, Wiedermann J, Lee C, et.al. Low voltage transmission electron microscopy of graphene. *Small*. 2015;11(5):515-542. DOI:10.1002/smll.201401804

34. De Rosa S, Branchini P, Yivlialin R, Duò L, Bussetti G, Tortora L. Disclosing the graphite surface chemistry in acid solutions for anion intercalation. *ACS Applied Nano Materials.* 2020;3(1):691-698. DOI:10.1021/acsanm.9b02220

Информация об авторах / Information about the authors

Белоногов Евгений Константинович, доктор физико-математических наук, доцент, профессор, ФГБОУ ВО «Воронежский государственный технический университет», Воронеж, Российская Федерация; ORCID 0000-0002-0216-0986;
e-mail: ekbelonogov@mail.ru

Кущев Сергей Борисович, доктор физико-математических наук, профессор, ФГБОУ ВО «Воронежский государственный технический университет», Воронеж, Российская Федерация; ORCID 0000-0003-1263-1806; e-mail: kushev_sb@mail.ru

Солдатенко Сергей Анатольевич, кандидат физико-математических наук, старший научный сотрудник, ФГБОУ ВО «Воронежский государственный технический университет», Воронеж, Российская Федерация; ORCID 0000-0002-3041-9959; e-mail: cossack408@mail.ru

Тураева Татьяна Леонидовна, кандидат физико-математических наук, доцент, ФГБОУ ВО «Воронежский государственный технический университет», Воронеж, Российская Федерация; ORCID 0000-0002-6126-1605; e-mail: tlturaeva@mail.ru

Evgeny K. Belonogov, D. Sc. (Physics and Mathematics), Associate Professor, Professor, Voronezh State Technical University, Voronezh, Russian Federation; ORCID 0000-0002-0216-0986;
e-mail: ekbelonogov@mail.ru

Sergey B. Kushev, D. Sc. (Physics and Mathematics), Professor, Voronezh State Technical University, Voronezh, Russian Federation; ORCID 0000-0003-1263-1806; e-mail: kushev_sb@mail.ru

Sergey A. Soldatenko, Cand. Sc. (Physics and Mathematics), Senior Researcher, Voronezh State Technical University, Voronezh, Russian Federation; ORCID 0000-0002-3041-9959; e-mail: cossack408@mail.ru

Tatiana L. Turaeva, Cand. Sc. (Physics and Mathematics), Associate Professor, Voronezh State Technical University, Voronezh, Russian Federation; ORCID 0000-0002-6126-1605; e-mail: tlturaeva@mail.ru

Received 27 September 2021; Accepted 12 November 2021; Published 28 December 2021